Long-range interactions between substitutional nitrogen dopants in graphene: electronic properties calculations

Philippe Lambin, Hakim Amara, François Ducastelle, Luc Henrard

Long-range interactions between substitutional nitrogen dopants in graphene: electronic properties calculations

Ph. Lambin,[1] H. Amara,[2] F. Ducastelle,[2] and L. Henrard[1]

[1] *Physics Department (PMR), University of Namur (FUNDP), B-5000 Namur, Belgium*
[2] *Laboratoire d'Etude des Microstructures, ONERA-CNRS, BP 72, 92322 Châtillon Cedex, France*

Being a true two-dimensional crystal, graphene has special properties. In particular, a point-like defect in graphene may have effects in the long range. This peculiarity questions the validity of using a supercell geometry in an attempt to explore the properties of an isolated defect. Still, this approach is often used in *ab-initio* electronic structure calculations, for instance. How does this approach converge with the size of the supercell is generally not tackled for the obvious reason of keeping the computational load to an affordable level. The present paper addresses the problem of substitutional nitrogen doping of graphene. DFT calculations have been performed for 9×9 and 10×10 supercells. Although these calculations correspond to N concentrations that differ by $\sim 10\%$, the local densities of states on and around the defects are found to depend significantly on the supercell size. Fitting the DFT results by a tight-binding Hamiltonian makes it possible to explore the effects of a random distribution of the substitutional N atoms, in the case of finite concentrations, and to approach the case of an isolated impurity when the concentration vanishes. The tight-binding Hamiltonian is used to calculate the STM image of graphene around an isolated N atom. STM images are also calculated for graphene doped with 0.5 at% concentration of nitrogen. The results are discussed in the light of recent experimental data.

PACS numbers: 73.22.Pr, 31.15.aq

I. INTRODUCTION

Local defects and chemical doping is a well-documented way to tune the electronic properties of graphene.[1] More specifically, the consequences of doping have been emphasized in the context of (bio)sensing,[2] lithium incorporation battery,[3,4] and in other fields. Nitrogen (N) is a natural substitute for carbon in the honeycomb structure due to both its ability to form sp^2 bonds and its pentavalent character. It is not a surprise, then, that many publications deal with the production of N-doped graphene realized either by direct growth of modified layers[5,6] or by post-synthesis treatments.[7,8] Doping of single wall nanotubes has also been considered.[9–11]

Recent STM-STS experiments of N-doped graphene[5,8] have demonstrated the occurrence of chemical substitution. These experiments provide us with a detailed and local analysis with sub-atomic resolution of the electronic properties of the doped material. The STM images display a pattern having three-fold symmetry around the N atoms and having a high contrast on the C atoms bonded to the dopant, which *ab-initio* simulations reproduce well.[12] STS measurements have revealed a broad resonant electronic state around the dopant position and located at an energy of 0.5 eV above the Fermi level.[8]

It is important to understand the effects of local defects and chemical doping on the global electronic properties of graphene, on its quantum transport properties and on its local chemical reactivity. It is the reason why the electronic properties of graphene doped with nitrogen have been investigated by several groups, mainly on the basis of *ab-initio* DFT techniques.[5,12–17] The strong advantage of the *ab-initio* approach is that it does not require any parametrization. A disadvantage is to be restricted to periodic systems as long as fast Fourier transforms need to be used to link direct and reciprocal spaces. In most instances, doping is therefore addressed in a supercell context, which forbids dealing with very low doping concentration or disorder. In the case of single wall nanotubes, however, the electronic properties of *isolated defects* have been studied by first-principle methods based on scattering theory.[18] For a nitrogen impurity in the (10,10) armchair nanotube, the local density of states on the N atom shows a broad peak centered at 0.53 eV above the Fermi level. The charge density associated with that quasi-bound state (donor level in the language of semiconductor physics) extends up to $\sim$1 nm away from the defect. This means that N atoms located $\sim$2 nm apart can interact, which requires examining with care the intrinsic validity of a supercell method.

The present work, based on both *ab-initio* DFT and semi-empirical tight-binding electronic structure calculations, aims at looking for interference effects generated by a distribution of N dopants in graphene as compared to the case of an individual impurity. We resort to different tight-binding parametrization strategies. The simplest one, based on just one adjustable parameter related to the defect, permits analytical calculations of the impurity levels. This model is described in the Appendix. We favor a more realistic approach, in which the perturbation induced by the defect is allowed to extend on the neighboring sites. This latter model is used to study the effects of disorder on the local and global electronic properties of doped graphene and to calculate STM images that we compare with available experimental data. The calculations and discussions are developed here for substitutional nitrogen. The conclusions would be qualitatively the same for boron doping and for other types

of point-like defects.

II. METHODOLOGY

The SIESTA package[19] was used for the *ab-initio* DFT calculations. The description of the valence electrons was based on localized pseudo-atomic orbitals with a double-ζ polarization (DZP).[20] Exchange-correlation effects were handled within local density approximation (LDA) as proposed by Perdew and Zunger.[21] Core electrons were replaced by nonlocal norm-conserving pseudopotentials.[22] Following previous studies,[8,12] the first Brillouin zone (BZ) was sampled with a 15×15 grid generated according to the Monkhorst-Pack scheme[23] in order to ensure a good convergence of the self-consistent electronic density calculations. Real-space integration was performed on a regular grid corresponding to a plane-wave cutoff around 300 Ry. All the atomic structures of self-supported doped graphene have been relaxed.

As mentioned above, the DFT calculations are based on a code that requires a periodic system. As a consequence, a supercell scheme have been applied for substitutionaly doped graphene. The atomic concentration of dopants is then directly related to the size of the supercell: 0.6 at% for a 9×9 supercell and 0.5 at% for a 10×10 supercell.

For the tight-binding parametrization, the following, well-established procedure was followed.[13–15] The Hamiltonian included the π electrons only, the hopping parameter between nearest-neighbor atoms was set to the *ab-initio* DFT value γ_0 = -2.72 eV. The same hopping was used between the N atom and its C first neighbors, which is not a severe approximation. It is indeed shown in the Appendix that a non-diagonal perturbation of the Hamiltonian can be offset by a renormalization of the N on-site energy, and this energy is a free parameter to be adjusted to the results of *ab-initio* calculations. The C on-site energies were assumed to vary with the distance d to the impurity according to a Gaussian law:

$$\varepsilon(d) = \varepsilon_C - |U| \exp(-0.5d^2/\sigma^2) \,, \qquad (1)$$

where $|U|$ is the depth of the potential well induced by the nitrogen (boron induces a potential hump, instead[13,24]) and ε_C is the asymptotic bulk value of the on-site parameter of carbon. ε_C defines the Dirac energy of pure graphene and has no other influence on the density of states (DOS) than a systematic shift of all the electronic levels. It will be set to zero, except otherwise specified. The standard deviation σ in eq. (1) was set to 0.15 nm, according to data of Ref. [24], whereas U was chosen so as to best fit DFT local DOS calculated on the N atom in the 9×9 supercell (see below).

In order to avoid the constraints of a periodic system, the local DOS have been computed with the recursion method.[25] 150 pairs of recursion coefficients were calculated on the computer. The coefficients were extrapolated to their asymptotic values related to the edges $\varepsilon_C \pm 3\gamma_0$ of the π bands of pure graphene. It is worth emphasizing than this procedure avoids to introduce any broadening of the energy levels. A drawback is the presence of wiggles that may be observed in some densities of states. They are sorts of Gibbs oscillations generated by the van Hove singularities, in particular by the abrupt discontinuities of the graphene π DOS at both band edges.

The present work aims at tailoring a simple tool for exploring the effects of the defect configurations. For that reason, achieving the best possible fit of DFT calculations for a specific supercell is superfluous. The following Sections illustrate the results obtained from the simple Gaussian model of eq. (1) based on the aforementioned values of the parameters U and σ.

III. PERIODIC DISTRIBUTION OF N

Fig. 1(a) shows DFT local densities of states on the N atom, on the first-neighbor atoms and on carbons located farther (0.5 – 0.7 nm) away, all in a 9×9 supercell. The important observation is the existence of two peaks, located at 0.55 and 0.92 eV above the minimum of the density of states (close to the Dirac point energy) in the N local DOS. A broadening of 0.05 eV on a 45×45 grid was used for the calculations.

For what concerns the electronic states associated with N doping in the unoccupied π band, the present DFT calculations are in overall good agreement with results published for 4×4,[13,16] 5×5,[17] 7×7,[5] and 10×10 supercells.[12] The double-peak structure in the local N DOS plotted in Fig. 1(a)) was not observed in previous calculations because of the large energy broadening that was used then,[5,12] except in Ref. [8]. It will be demonstrated below that the observed double-peak structure is a consequence of long-range interactions between the N impurities that were reproduced periodically in the graphene sheet because of the supercell geometry.

Fig. 1(b) shows tight-binding densities of states of the same 9×9 supercell after Lorentzian broadening, aimed at facilitating the comparison with the DFT results, and application of an energy shift (ε_C = -0.25 eV) bringing the minimum of the DOS at the position it has in Fig. 1(a). The DTF results are qualitatively well reproduced by the π-electron tight-binding Hamiltonian by taking $|U|$ = -4 eV in eq. (1). By comparison, the on-site energies in Ref. [14] can be approximated by a sum of two Gaussians, $\varepsilon(d) = \varepsilon_C - 2.95 \exp(-0.5d^2/\sigma_1^2) - 0.59 \exp(-0.5d^2/\sigma_2^2)$ (in eV), with σ_1 = 0.10 nm and σ_2 = 0.39 nm. The second term has a longer range than the single Gaussian law used in the present calculations, and the potential well at the N location is about 10% shallower than here.

The tight-binding densities of states of the same 9×9 superstructure as in Fig. 1, now calculated without energy broadening, are displayed in Fig. 2(a). A substructure clearly emerges where the broadened local DOS only

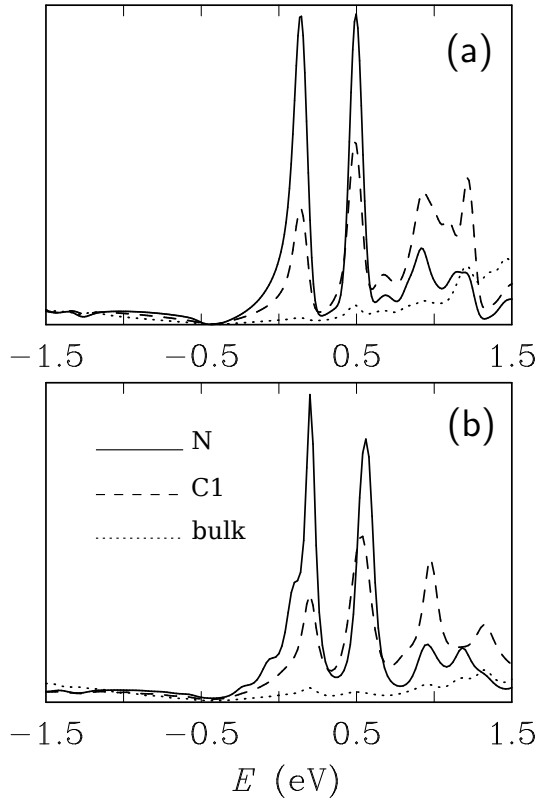

FIG. 1. (a) DFT and (b) tight-binding local densities of states of graphene doped with N at a concentration of one impurity per 9×9 supercell (162 atoms). The different curves represent the local DOS on the N atom, on the first-neighbor carbons (C1), and on a few distant carbons (bulk).

showed the double-peak feature discussed here above. In addition, Fig. 2(a) reveals that there are much less electronic states in the region between 0 and 1.5 eV on the second-neighbor atoms (C2) than on the first- (C1) and third-neighbor (C3) carbons (see Fig 2(b) for the notations). The same observation as for C2 can be made for the local DOS on the fourth neighbors (not shown). This oscillation between lower and higher densities of states brings out the fact that the two sublattices of graphene are differently affected by a substitutional defect (see also the Appendix).

The reliability of the tight-binding calculations compared to DFT can be appreciated from Figs. 2(c,d) that come from the 10×10 supercell (0.5 at% concentration of N). The good agreement between the two approaches reinforces the fact that the parametrization of the on-site energies used for the 9×9 supercell describes well the doped graphene systems and does not require further adjustment depending on the actual concentration and environment. Electronic states localized on and near the N dopant are observed within 1.5 eV from the Dirac energy, as for the 9×9 supercell. However, the multi-peak structure in the local N DOS of 10×10 (Fig. 2(c)) is totally different from that of 9×9 (Fig. 2(a)), despite similar N concentrations (0.5 at% and 0.6 at%, respectively). This finding is a clear indication of the importance of interference effects among the supercells.

The band structure of the DFT calculations (not shown) provides us with another difference between the two superstructures: the 10×10 N-doped superstructure has a direct band gap of 0.05 eV at the K point of its Brillouin zone, whereas the the 9×9 N-doped superstructure has no gap. The zero of energy of the DFT local DOS shown in Fig. 2(d) was positioned at the center of the gap, the Fermi level being 0.3 eV higher.

In the tight-binding calculations, the band gap of the 10×10 superstructure is located 0.14 eV below the Dirac point of pure graphene (ε_C, set to zero in Fig. 2(a,c)). The Fermi level E_F of the doped superstructures was found to lie 0.27 eV and 0.25 eV above ε_C for the 9×9 and 10×10 systems, respectively, which means 0.43 eV and 0.39 eV above the minimum of the DOS (the corresponding DFT values are 0.42 and 0.36 eV, respectively). The σ bands below the Fermi energy are completely filled, the π bands of the supercell must accommodate an extra electron brought about by the nitrogen. The occupied local π DOS of the N atom contains 1.36 electron in both the 9×9 and 10×10 supercells. The remaining 0.64 excess electron is distributed on the surrounding carbons, of which a total of 0.56 sits on the three first neighbors (C1), which are therefore negatively charged.

For both 9×9 and 10×10 doped supercells, there is a localized state expelled from the π band and located 9.35 eV below E_F, to be compared with 8.65 eV in DFT calculations. This localized state weights more than 25% (0.57 state of the N local DOS, which can accommodate 2 electrons including the spin degeneracy). The large value of the weight can be understood from the arguments developed in the Appendix for a simplified tight-binding Hamiltonian.

We conclude here that the supercell technique would require a large cell if it were desired to describe the electronic states of an isolated dopant. In other words, the supercell technique is badly convergent when the size of the cell increases, particularly in low dimensions. The corresponding long range of a local perturbation produces interferences between the images of the defect generated by the periodic boundary conditions (see also Ref. [26]).

IV. ISOLATED N IMPURITY

We now turn our attention to the case of an isolated N impurity studied by tight-binding. The local DOS on and around an isolated N impurity are presented in Fig. 3. The calculations were performed on a 150x150 cell of graphene (45,000 atoms) with periodic boundary conditions. By restricting the number of pairs of recursion coefficients to 150, the impurities located in adjacent cells do not feel each other, which means that the N atoms are virtually isolated. In the N local DOS, there

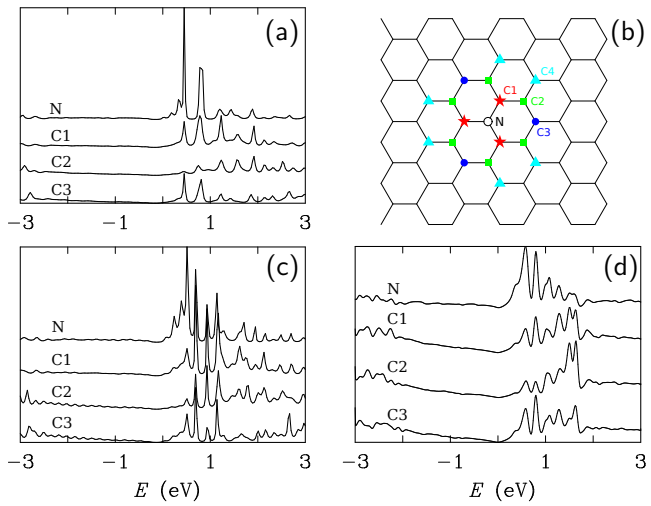

FIG. 2. (a) Tight-binding local DOS of the 9×9 superstructure without energy broadening. The labels, represented in panel (b), correspond to the nitrogen dopant (N), the first, second and third neighbors (C1, C2 and C3). (c) Tight-binding and (d) DFT local π densities of states on and around a substitutional N atom in graphene with 10×10 periodic distribution (200 atoms per cell). The curves have been shifted vertically for clarity.

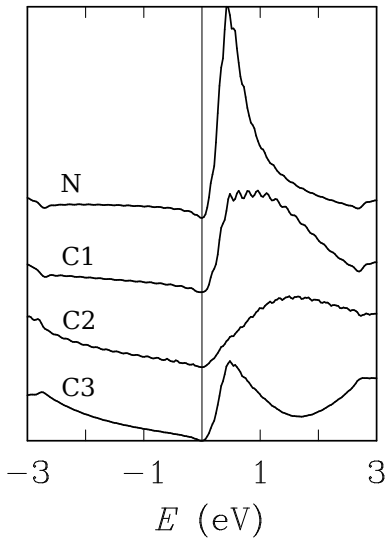

FIG. 3. Tight-binding local π densities of states on and around an isolated impurity in graphene. The labels correspond to the defect site (N), the first, second and third neighbors (C1, C2 and C3). The curves have been shifted vertically for clarity.

is a tall asymmetric peak located 0.5 eV above the Dirac energy (ε_C) of graphene. The peak broadens and shifts to 1 eV on the first neighbors and moves up further to 1.5 eV on the second neighbors. The local DOS on the third-neighbor atoms reproduces the resonance peak of the impurity, with a smaller amplitude. The local DOS on fourth neighbors (not shown) bears resemblance with that of pure graphene. It is interesting to observe in Fig. 3 that there remains almost nothing of the van Hove singularities of graphene at $\varepsilon_C \pm \gamma_0$ on the N and C1 sites.

The problem of an isolated impurity in graphene can be addressed analytically if one simplifies the Hamiltonian to a point-like defect by ignoring the Gaussian delocalization of the perturbation ($\sigma \to 0$ in eq. (1)). Details are presented in the Appendix. If this simple model captures the essential physics of the problem, it fails in producing the details brought about by the delocalized nature of the perturbation. As shown in the Appendix, perturbing the first-neighbor C atoms, in addition of course to the substitution site, leads to a better picture.

V. RANDOMLY DISTRIBUTED N ATOMS

Experimentally, nitrogen doping of graphene leads to randomly distributed substitutional sites,[5,8] with perhaps some preference of the dopant atoms to sit on the same sublattice, at least locally.[5] The calculations illustrated in the present Section were performed for nitrogen distributed randomly with an atomic concentration of 0.5%, identical to that realized with the 10×10 superstructure. The selection of the substitutional sites was constrained by the requirement that the distance between two nitrogens remains larger than $12\sigma = 1.8$ nm (see eq. (1)). The reason for that was to avoid any overlapping of the potential wells generated by the dopants.

Fig. 4 shows a configurational averaging of the local densities of states when the N atoms have equal probabilities to sit on one or the other of the graphene sublattices. This case will be referred to as "unpolarized" (or "uncompensated").[27] By configurational averaging, it is meant the arithmetic average of local DOS on 50 nitrogens selected randomly — among the 225 atoms that the 150x150 sample box contains — and the arithmetic average of local DOS on 150 randomly-selected C1, C2 and C3 sites. The N, C1, C2, and C3 average local DOS for the unpolarized disordered distribution all have a real and remarkable similarity with the ones obtained for an isolated impurity (Fig. 3). The result are in agreement with N local DOS for randomly distributed impurities obtained by Lherbier *et al.*[15] with a small broadening.

When the N atoms are put, still randomly, on the *same sublattice*, the multi-peak structure characteristics of the superlattice (see Fig. 2) reappears on the average local DOS, which are shown in Fig. 5. Interestingly, the local DOS on the second-neighbor atoms (C2), which belongs to the same sublattice as the N atom they surround, are virtually the same in Figs. 4 and 5, insensitive to the polarization of the N distribution. It is interesting to remark that, like with the 10×10 superstructure, there is a tiny gap of states 0.1 eV below the Dirac energy. The gap looks narrower in case of the unpolarized distribution compared to the polarized one. In the polarized case, the appearance of a gap is natural since the average diagonal

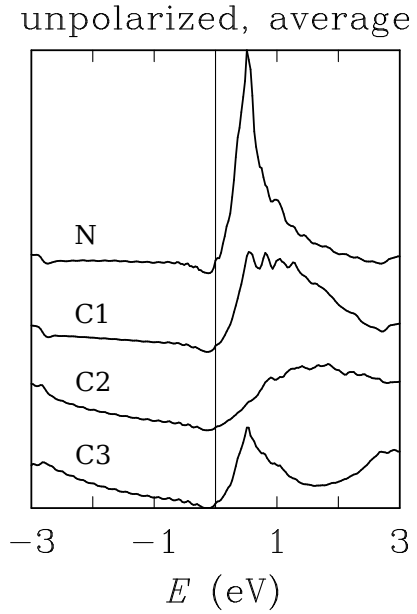

FIG. 4. Configurational average of the local π densities of states on and around substitutional N atoms in a graphene sheet containing 0.5 at% of nitrogen atoms randomly distributed on the two sublattices. The labels correspond to the nitrogen dopant (N), the first, second and third neighbors (C1, C2 and C3). The curves have been shifted vertically for clarity.

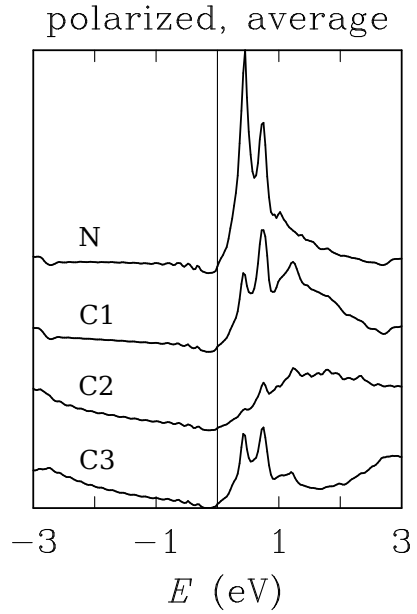

FIG. 5. Configurational average of the local π densities of states on and around substitutional N atoms in a graphene sheet containing 0.5 at% of nitrogen atoms randomly distributed on the *same sublattice*. The labels correspond to the nitrogen dopant (N), the first, second and third neighbors (C1, C2 and C3). The curves have been shifted vertically for clarity.

potential breaks the symmetry between the two sublattices. Similar effects have been observed in the case of vacancies.[27]

Averaging the local densities of states made the distinction between unpolarized and polarized distributions of N rather apparent. However, for a given configuration of the dopant atoms, the local DOS varies from site to site. How much that variation can be is illustrated in Fig. 6 that compares local DOS calculated on three different N atoms for both the unpolarized and the polarized distributions. The variations from site to site are so important that the local DOS is not a reliable indicator of the global distribution of the nitrogen atoms among the two sublattices. If it is true that the N local DOS displayed in Fig. 6 are less peaked that the N local DOS of the 10×10 superstructure (Fig 2), identifying which is which would be difficult on the experimental side if one had only STS spectra to deal with.

VI. STM IMAGES

A reliable information on the electronic structure of doped graphene can be obtained by STM imaging. A tip polarized negatively compared to the graphene layer probes the unoccupied states where a N substitutional impurity and the adjacent carbon atoms have peaks in their local DOS. The increase of electronic density of states, compared to graphene, in this energy region gives rise to a bright triangular spot in the STM image,[5,8,12,17] with two possible orientations with respect to the honeycomb lattice depending on the sublattice on which the N dopant sits. These two orientations are rotated by 180° from each other, as observed experimentally.[5,8]

Fig. 7 is a tight-binding STM image[28] computed for graphene with a single N impurity. The prominent triangular arrow-head at the center of the image is located on the N, C1 and C3 sites. The second-neighbor carbons (C2) atoms do not participate much to the STM signature of the dopant. This is so because the local DOS in the energy window probed by the STM current (0 to 0.5 eV) is significantly smaller on the C2 atoms than on the N, C1 and C3 atoms (see Fig. 3).

Fig. 8 shows two STM images computed for graphene doped with N at 0.5 at% concentration, the dopants being randomly distributed on the two sublattices. In the configuration shown in the left-hand side image, there are two impurities located 1.9 nm apart sitting on the same sublattice. The two nitrogens captured in the right-hand side images do not sit on the same sublattice, which explains why the related triangular STM patterns are oriented differently. The scale used for the STM signal (tip height at constant current) is identical for both images. For improving the contrast, the scale has been saturated below 4.0 Åand above 5.8 Å. Two dopants seem to interfere more when they are located on the two sublattices than when they sit on the same sublattice.

In tight-binding STM theory,[28] there is an empirical

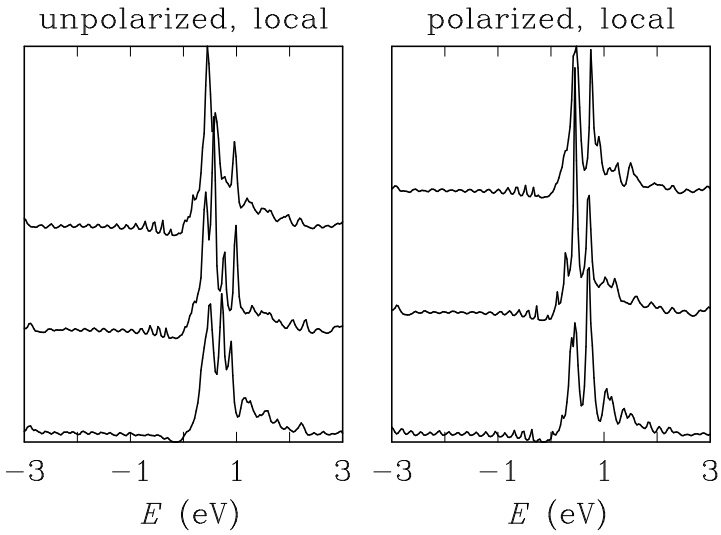

FIG. 6. Local DOS on three N atoms randomly selected in graphene doped at concentration 0.5 at%. The unpolarized case (left) refers to dopants located on the two sublattices, whereas the dopants all sit on the same sublattice in the polarized case (right).

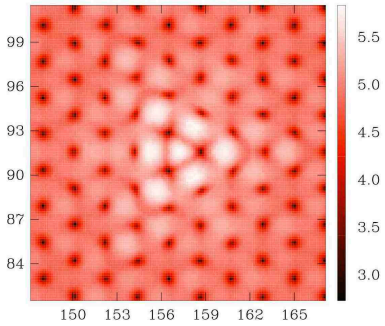

FIG. 7. Computed tight-binding STM image of graphene with an isolated N impurity located at coordinates 157.2, 91.6 (all positions are in Å) for a negatively-polarized tip ($V_{\rm tip}$ = -0.5 V).

parameter coupling the tip apex to the sample atoms, which was chosen independent of the chemical nature of the probed atoms. In other words, the STM calculations differentiate a N atom from the C atoms only through intrinsic effects that the former has on the electronic structure of the doped graphene. In DFT calculations, the standard way to generate an STM image is via Tersoff-Hamann's theory.[29] In addition to local variations of the DOS, the tunnel current depends on the spatial extension of the π orbitals in the direction perpendicular to the atomic plane. The $2p_z$ orbital of N decreases more rapidly than the $2p_z$ orbital of C does,[12] which means that the contrast of the computed image depends on the tip–sample distance. This dependence is illustrated in Figs. 9(a) and (b) that represent DFT constant-current STM images computed for a small current (large tip-sample distance) and for a large current

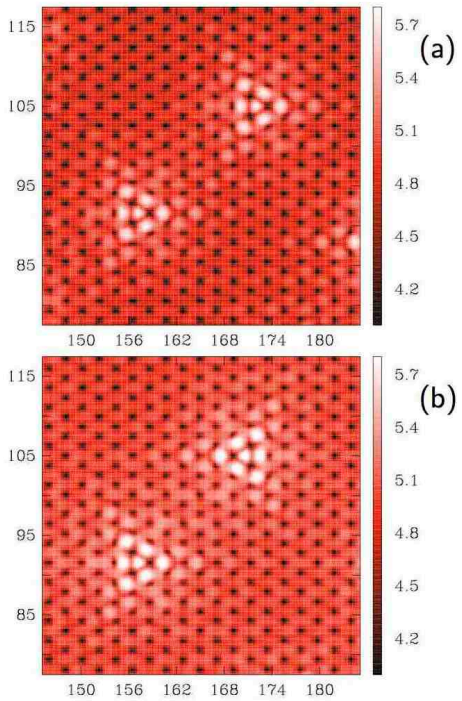

FIG. 8. Constant-current STM images computed for two configurations of graphene doped with 0.5 at% N. The distribution of the N atoms is random. The STM tip is polarized at -0.5 V compared to the sample.

(small tip-sample distance), respectively. The local DOS is larger on top of the N atom than on the top of all the other atoms, but it decreases much more rapidly in the normal direction. This explains the small brightness of the N site for the large tip–sample distance. Experimentally, variations of the STM contrast have also been observed as a function of the current/voltage conditions,[8] where image of the dopant atom protrudes in some occasions and does not in other occasions. It is tempting to attribute this observation to variations of the tip–sample distances depending on the current setpoint, as in Fig. 9. However, the experimental distance is much larger that the one that can be achieved numerically in DFT, due to the fast decay of the localized basis set when moving away from the sample surface.

VII. CONCLUSIONS

Tight-binding and DFT electronic calculations reveal that the perturbation induced by N dopants in graphene is long ranged. This is not a surprise when one remembers that the Green function of the free-electron problem in two dimensions is the Bessel-Hankel function of zeroth order $(i/4)H_0^{(1)}(k|\vec{r}-\vec{r}'|)$, which slowly decreases like $1/\sqrt{kd}$ with the distance $d=|\vec{r}-\vec{r}'|$, where $k=\sqrt{\hbar^2/2mE}$. For the π-electron tight-binding Hamiltonian on the honeycomb lattice, the Green function el-

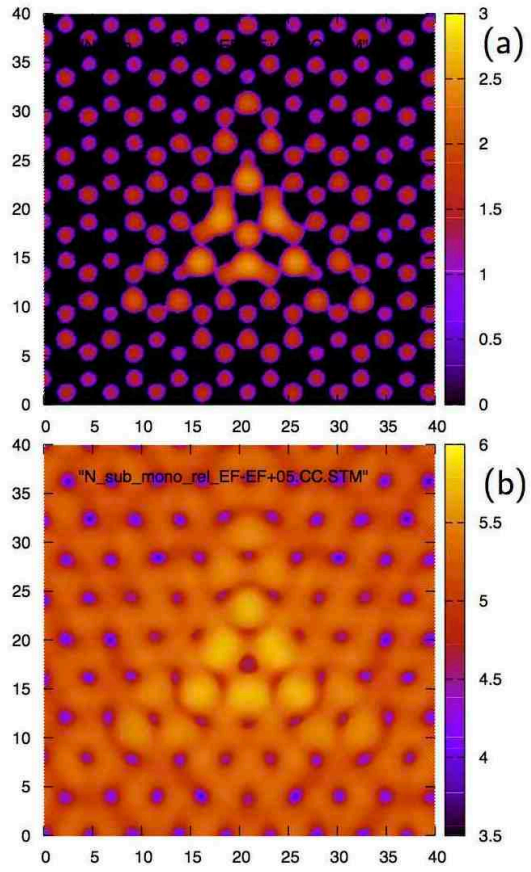

FIG. 9. DFT calculation of constant-current STM images of 10×10 N-doped graphene for two levels of the tunnel current: (a) high and (b) low.

ements G^0_{nm} can also be approximated, at low energy, by Hankel functions of $q|\vec{r}_m - \vec{r}_n|$, now of order zero or one, depending on whether they refer to sites m and n located on the same sublattice or not.[30] In this regime, the energy E is linearly related to q by the dispersion relation $E = \hbar v_F q$, where v_F is the Fermi velocity, and the Hankel functions are also multiplied by the energy and by periodic functions describing $\sqrt{3} \times \sqrt{3}$ modulations related to the Dirac wave vectors $\pm K$. For large separation distances, the Green function elements vary therefore like $1/\sqrt{E\,|\vec{r}_m - \vec{r}_n|/\hbar v_F}$, except for very small excitation energies where the Hankel functions diverge. A more detailed discussion will be given elsewhere.[31]

The scattering formalism developed in the Appendix for the case of a point-like defect emphasizes the central role of the Green function in the understanding of the perturbation induced by the defect. Hence the long-range interaction between dopants in graphene. It is important to realize that this long-range interaction is not the consequence of using an extended perturbation of the on-site energies around the defect (eq. (1)). Things actually go the other way round: a defect perturbs the crystal potential far away, because of the slow decay of the scattering it produces. As a consequence, the parameters of the tight-binding Hamiltonian that mimic *ab-initio* calculations are affected in some neighborhood of the defect.[14]

This long-range interaction has several effects. First, it produces interferences between the duplicates of the defect generated by periodic boundary conditions when a supercell approach is used. The latter must therefore be used with caution. Second, substitutional defects dispersed in graphene cannot be treated as independent as soon as the distance between two of them becomes smaller then, say, 2 nm. Shallow defects are expected to be less sensitive to mutual interactions than deeper ones, the deepest defect being the vacancy. As shown in the Appendix, nitrogen, with its 10 eV effective perturbation parameter, is not a shallow defect. Boron would not be shallow either. Thus increasing the strength of the local potential also increases the range of the perturbation it produces. This unusual behavior is actually related to the behavior of the Green functions at low energy (see Appendix and Refs. [32, 33, 34]). As a consequence, the STM image of a defect in graphene may be influenced by the proximity of another defect. What happens when two impurities come very close to each other remains to be clarified. A new parametrization of the tight-binding Hamiltonian, depending on the N-N distance, is required.

As demonstrated experimentally, the partition of the honeycomb network in two sublattices has subtle effects on STM image of graphene with substitutional dopants. It is again something that naturally comes out of the calculations, as exemplified by Fig. 8. Finally, it may be important to remark that the minimum of the π density of states around the N dopants does not coincide with the atomic level ϵ_C of carbon in graphene (the Dirac point energy; see also Refs [27, 33, 35]). Depending on the concentration, the DOS minimum shifts slightly below ϵ_C (see e.g. Fig. 5).

Acknowledgments This research has used resources of the Interuniversity Scientific Computing Facility located at the University of Namur, Belgium, which is supported by the F.R.S.-FNRS under convention No. 2.4617.07 and the FUNDP.

APPENDIX. THE IMPURITY PROBLEM IN GRAPHENE

Assuming that the on-site energies all take the bulk value $\varepsilon_C = 0$, except on the nitrogen atom where $\varepsilon_N = U$, the tight-binding Hamiltonian can be written in the form:

$$H = H^0 + V = -\sum_{n,m} |n\rangle t_{nm} \langle m| + |0\rangle U \langle 0| \,. \qquad (2)$$

The states $|n\rangle$ denote π orbitals centered on sites n: $\varphi_\pi(r - n) = \langle r|n\rangle$. H^0 is the usual tight-binding Hamiltonian where only hopping integrals $t_{nm} \equiv \gamma_0$ between first neighbors n and m are kept, and V is the localized potential of the N atom at site 0. The local density of

states $n(r,E)$ is given by:

$$n(r,E) = \sum_{n,m} n_{nm}(E)\varphi_\pi(r-n)\varphi_\pi(r-m)\ , \qquad (3)$$

where $n_{nm}(E)$ is obtained from the Green function or resolvent $G(z) = (z-H)^{-1}$:

$$n_{nm}(E) = \frac{-1}{\pi} \lim_{\varepsilon\to 0} \mathrm{Im}\ \langle n|G(E+i\varepsilon)|m\rangle\ . \qquad (4)$$

$G(z)$ can then be calculated in terms of the unperturbed Green function $G^0(z) = (z-H^0)^{-1}$; this is the so-called Koster-Slater-Lifshitz problem. If the matrix elements $\langle n|G(E+i\varepsilon)|m\rangle$ are written $G_{nm}(z)$, we have:

$$G_{nm} = G^0_{nm} + G^0_{n0}\tau G^0_{0m} \quad ; \quad \tau = \frac{U}{1-UG^0_{00}}\ . \qquad (5)$$

In particular, on the impurity site, we have $G_{00} = G^0_{00}/(1-UG^0_{00})$,[36,37] and the local density of states on the N site, $n_N(E) \equiv n_{00}(E)$ is given by:

$$n_N(E) = \frac{n^0(E)}{(1-UF^0(E))^2 + \pi^2U^2n^0(E)^2}\ , \qquad (6)$$

where $F^0(E)$ is the real part of the Green function $G^0_{00}(E+i\varepsilon)$, *i.e.* the Hilbert transform of the unperturbed density of states of graphene $n^0(E)$.

Close to the Dirac point, $n^0(E) \sim |E|$ and $F^0(E) \sim E\ln|E|$, and provided U is large enough, $n_N(E)$ shows a resonant behavior around the energy E_r such that $(1-UF^0(E_r)) = 0$ (see the open-circle symbol in Fig. 10). This has been discussed in many places.[27,30,32,35,38–40] It turns out that a value for U of the order of -10 eV reproduces a resonance at the position obtained with the previous model (compare Fig. 11(a) with Fig. 3) instead of the value $U = -4$ eV in the previous approach. However, the shapes of the local DOS differ to some extent between both tight-binding models. The resonance here (Fig. 11(a)) is weaker on the N site than on the sites C1 and C3 located on the other sublattice, which can be explained from the symmetry properties of the unperturbed Green functions: $G_{nm}(z)$ is and odd or even function of z depending on sites n and m belonging to the same sublattice of the graphene structure or not. As a consequence, for example, $G^0_{00}(z=0) = 0$ whereas the real part of $G^0_{0n}(z=0)$ does not vanish when n is a first neighbor, which has a big impact on the local densities of states (see eq. (5)).[31] Also the van Hove singularities at 2.7 eV are still present here.

In addition to the *resonant* state located above the Dirac point, Fig. 10 reveals the existence of a *localized* state lying below the π-electron DOS, where the on-site perturbation level $1/U$ intersects the curve $F^0(E)$ at -4.5$|\gamma_0|$ (solid square symbol). The weight (residue) of this localized state is inversely proportional to the slope of $F^0(E)$ at the intersection. This is the localized state found at 9.35 eV below E_F in tight-binding and 8.65 eV below E_F in DFT calculations for the doped superstructures (Section III).

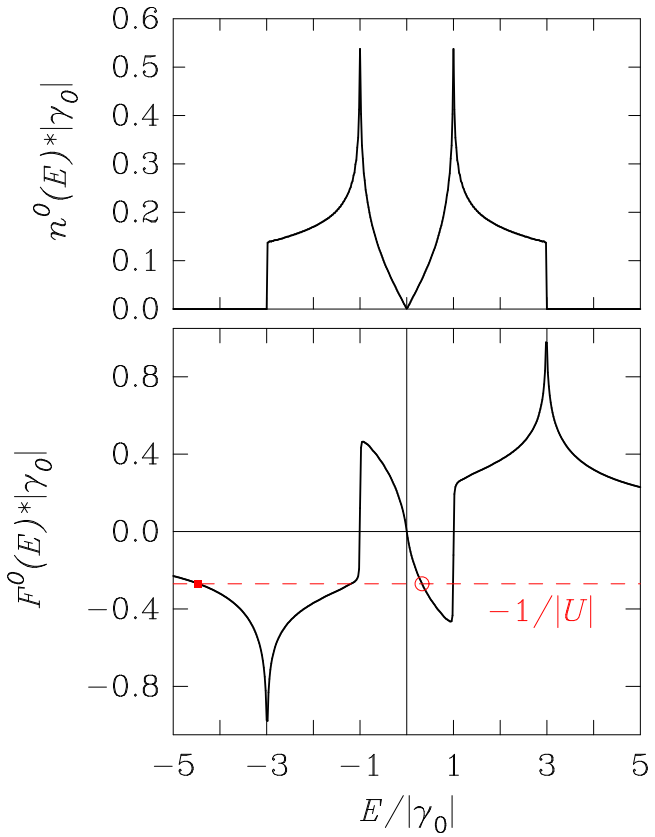

FIG. 10. Real ($F^0(E)$) and imaginary ($n^0(E)$) parts of the Green function of the graphene π tight-binding Hamiltonian along the real axis, in units of $|\gamma_0|$. The intersection of $F^0(E)$ with the reciprocal of the perturbed level $1/U$ (dashed line) in the vicinity of the Dirac point gives the energy E_r at which the local DOS of the impurity has a resonance (open circle symbol). There is another intersection (filled symbol) giving rise to a localized state below the π-electron density of states.

This one-parameter model can be generalized to other type of local defects or chemical doping. B doping, with a positive U, is almost symmetrical to N doping. The limit $U \to \infty$ corresponds to the introduction of a vacancy instead of a substitutional impurity. Because of the vanishing of the density of states and of the logarithmic divergence of $F^0(E)$, this limit is singular and must been studied with special care.[27,35,39–41] The resonant state becomes very narrow, but does not become a genuine bound state. The total density of states varies as $1/([\ln|E|]^2|E|)$ and the perturbation of the electronic density is concentrated on the first neighbors and on the sites belonging to the sublattice different from that of the vacancy.[31]

The simple model developed here above allows one to address the question of the role of N-C hopping interactions on the local DOS on the impurity. When the N-C hopping takes a value γ different from the one γ_0 between the C atoms, the Green function element on the

perturbed site can be set in the form

$$G_{00}(z) = \frac{1}{z - U - (\gamma^2/\gamma_0^2)\Sigma^0(z)} \ , \qquad (7)$$

where $\Sigma^0(z)$ is the self energy of the unperturbed graphene. In the notations of the above formalism, the self energy can be identified to $\Sigma^0(z) = z - 1/G_{00}^0(z)$. Inserting this expression in the right-hand side of eq. (7) leads to a generalization of eq. (6) valid for $\gamma \neq \gamma_0$. In particular, the resonance condition in the vicinity of $E = 0$ becomes

$$\frac{\gamma^2}{\gamma_0^2 U + (\gamma^2 - \gamma_0^2)E_r} = F^0(E_r) \ . \qquad (8)$$

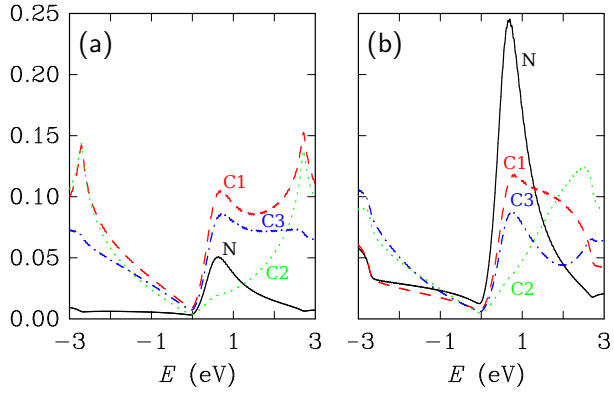

FIG. 11. Local densities of states deduced from the simple tight-binding model for an isolated nitrogen impurity in graphene. (a) On-site perturbation energy U = -10 eV on the N site only; (b) on-site perturbation on the N (-4 eV) and the three C1 sites (-2.57 eV).

By comparison with the situation depicted in Fig. 10, the intersection of $F^0(E)$ needs now to be search for with a curve whose ordinate and slope at the origin are $-\gamma^2/(\gamma_0^2|U|)$ and $\gamma^2(\gamma_0^2 - \gamma^2)/(\gamma_0^2 U)^2$, respectively. If $|\gamma| < |\gamma_0|$, which should be the case here since the N atom is smaller than the C one, the ordinate at the origin of the curve moves up and its slopes becomes positive. These two effects pull the resonant energy E_r closer to the origin compared with the simplest situation where $|\gamma| = |\gamma_0|$. However, if the hopping perturbation is small, renormalizing the on-site level U to a larger absolute value $U_{\rm eff}$ would produce the same effect. This conclusion validates the approach used so far to not modifying the N-C hopping.

We have finally considered an intermediate model between the Gaussian distribution of the on-site energies and the one-parameter model just described. We took U_0 on the N site and a second perturbation potential U_1 on the first neighbors, with values fixed by eq. (1), $U_0 = -4$ eV; $U_1 = -2.57$ eV. The agreement with the full Gaussian model is much better than with the one parameter model (Fig. 11(b)). It is fairly remarkable to realize that the intensity of the resonance state on the N site increases when the potential is delocalized on the first neighbors.

[1] S. Niyogi, E. Bekyarova, J. Hong, S. Khizroev, C. Berger, W. de Heer, and R.C. Haddon, J. Phys. Chem. Lett. **2**, 2487 (2011).
[2] Y. Wang, Y. Shao, D.W. Matson, J. Li, and Y. Lin, ACS Nano **4**, 1790 (2010).
[3] A.L.M. Reddy, A. Srivastava, S.R. Gowda, H. Gullapall, M. Dubey, and P.M. Ajayan, ACS Nano **4**, 6337 (2010).
[4] Y. Li, J. Wang, X. Li, D. Geng, M.N. Banis, R. Li, and X. Sun, Electroch. Comm. **18**, 12 (2012).
[5] L. Zhao, Rui He, Kwang Taeg Rim, Th. Schiros, Keun Soo Kim, Hui Zhou, C. Gutiérrez, S.P. Chockalingam, C.J. Arguello, L. Pálová, D. Nordlund, M.S. Hybertsen, D.R. Reichman, T.F. Heinz, Ph. Kim, A. Pinczuk, G.W. Flynn, and A.N. Pasupathy, Science **333**, 999 (2011).
[6] Y. Wei, Y. Liu, Y. Wang, H. Zhang, L. Huang, and G. Yu, Nano Lett. **9**, 1752 (2009).
[7] B. Guo, Q. Liu, E. Chen, H. Zhu, L. Fang, and J.R. Gong, Nano Lett. **10**, 4975 (2010).
[8] F. Joucken, Y. Tison, J. Lagoute, J. Dumont, D. Cabosart, Bing Zheng, V. Repain, C. Chacon, Y. Girard, A.R. Botello-Mendez, S. Rousset, R. Sporken, J.C. Charlier, and L. Henrard, Phys. Rev. B **85**, 161408 (2012).
[9] R. Arenal, X. Blase, and A. Loiseau, Advances in Physics **59**, 101 (2010).
[10] P. Ayala, R. Arenal, A. Loiseau, A. Rubio, and T. Pichler, Rev. Mod. Phys. **82**, 1843 (2010).
[11] H. Lin, J. Lagoute, V. Repain, C. Chacon, Y. Girard, J.S. Lauret, R. Arenal, F. Ducastelle, S. Rousset, and A. Loiseau, Comptes Rendus Physique **12**, 909 (2011).
[12] B. Zheng, P. Hermet, and L. Henrard, ACS Nano **7**, 4165 (2010).
[13] S. Latil, S. Roche, D. Mayou, and J.C. Charlier, Phys. Rev. Lett. **92**, 256805 (2004).
[14] C. Adessi, S. Roche, and X. Blase, Phys. Rev. B **73**, 125414 (2006).
[15] A. Lherbier, X. Blase, Y.M. Niquet, F. Triozon, and S. Roche, Phys. Rev. Lett. **101**, 036808 (2008).
[16] Y. Fujimoto and S. Saito, Phys. Rev. B **84**, 245446 (2011).
[17] W.H. Brito, R. Kagimura, and R.H. Miwa, Phys. Rev. B **85**, 035404 (2012).
[18] H.J. Choi, J. Ihm, S.G. Louie, and M.L. Cohen, Phys. Rev. Lett. **84**, 2917 (2000).
[19] D. Sánchez-Portal, P. Ordejón, E. Artacho, and J. M. Soler, Int. J. Quantum Chem. **65**, 453 (1997).
[20] E. Artacho, D. Sánchez-Portal, P. Ordejón, A. García, and J.M. Soler, Phys. Status Solidi b **215**, 809 (1999).
[21] J.P. Perdew and A. Zunger, Phys. Rev. B **23**, 5048 (1981).
[22] N. Troullier and J.L. Martins, Phys. Rev. B **43**, 1993 (1991).
[23] H.J. Monkhorst and J.D. Pack, Phys. Rev. B **13**, 5188 (1976).
[24] H. Khalfoun, P. Hermet, L. Henrard and S. Latil, Phys.

Rev. B **81**, 193411 (2010).
[25] R. Haydock, V. Heine and M.J. Kelly, J. Phys. C Solid St. Phys. **8**, 2591 (1975).
[26] Z. Zanolli and J.C. Charlier, Phys. Rev. B **81**, 165406 (2010).
[27] V.M. Pereira, J.M.B. Lopes dos Santos, and A.H. Castro Neto, Phys. Rev. B **77**, 115109 (2008).
[28] V. Meunier and Ph. Lambin, Phys. Rev. Lett. **81**, 5588 (1998).
[29] J. Tersoff and D.R. Hamann, Phys. Rev. Lett. **50**, 1998 (1983).
[30] Z.F. Wang, Ruoxi Xiang, Q.W. Shi, Jinlong Yang, Xiaoping Wang, J.G. Hou, and Jie Chen, Phys. Rev. B **74**, 125417 (2006).
[31] F. Ducastelle *et al*, unpublished (2012).
[32] Y.V. Skrypnyk and V.M. Loktev, Phys. Rev. B **73**, 241402 (2006).
[33] S.S. Pershoguba, Y.V. Skrypnyk, and V.M. Loktev, Phys. Rev. B **80**, 214201 (2009).
[34] Y.V. Skrypnyk and V.M. Loktev, Phys. Rev. B **83**, 085421 (2011).
[35] Shangduan Wu, Lei Jing, Qunxiang Li, Q.W. Shi, Jie Chen, Haibin Su, Xiaoping Wang, Jinlong Yang, Phys. Rev. B **77**, 195411 (2008).
[36] G.F. Koster and J.C. Slater, Phys. Rev. **95**, 1167 (1954).
[37] I.M. Lifshitz, Sov. Phys. Usp. **7**, 549 (1965).
[38] T.O. Wehling, A.V. Balatsky, M.I. Katsnelson, A.I. Lichtenstein, K. Scharnberg, R. Wiesendanger, Phys. Rev. B **75**, 125425 (2007).
[39] A. Toyoda and T. Ando, J. Phys. Soc. Japn **79**, 094708 (2010).
[40] Yi Chen Chang and S. Haas, Phys. Rev. B **83**, 085406 (2011).
[41] Sh. Yuan, H. De Raedt, M.I. Katsnelson, Phys. Rev. B **82**, 115448 (2010).